Chemistry Letters, 2025, **54**, upaf130
https://doi.org/10.1093/chemle/upaf130
Advance access publication 7 July 2025

Letter

Temperature-modulated molten salt synthesis of FeNi alloy/carbon electrocatalyst for enhanced oxygen evolution reaction

Xueda Liu[1], Dongyuan Song[1], Liyuan Dai[1], Keqiang He[1], Takeshi Yanagida[2], Johnny C. Ho[3,4], SenPo Yip[4,*]

[1]Interdisciplinary Graduate School of Engineering Sciences, Kyushu University, 6-1 Kasuga Koen, Kasuga, Fukuoka 816-8580, Japan

[2]Department of Applied Chemistry, Graduate School of Engineering, The University of Tokyo, 7-3 Hongo, Bunkyo City, Tokyo 113-8656, Japan

[3]Department of Materials Science and Engineering, City University of Hong Kong, 83 Tat Chee Ave, Kowloon Tong, Kowloon, Hong Kong SAR 999077, P. R. China

[4]Institute for Materials Chemistry and Engineering, Kyushu University, 6-1 Kasuga Koen, Kasuga, Fukuoka 816-8580, Japan

*Corresponding author: Institute for Materials Chemistry and Engineering, Kyushu University, 6-1 Kasuga Koen, Kasuga, Fukuoka 816-8580, Japan. Email: yip.sen.po.472@m.kyushu-u.ac.jp

Abstract

In this study, FeNi alloy/carbon composites were synthesized using the LiCl–KCl molten-salt-assisted method at different temperatures. Electrochemical tests demonstrate that FeNi/carbon synthesized at 1,000 °C exhibits the best oxygen evolution reaction performance, with an overpotential of 306.7 mV at a current density of 10 mA cm^{-2} and excellent long-term stability over 100 h. A series of characterizations reveals that the improved activity is attributed to the synergistic effects of the conductive and porous carbon framework, the well-grown FeNi alloy nanoparticles, and optimized surface electronic states that derive from the increasing calcination temperature.

Keywords: molten salt synthesis, oxygen evolution reaction, temperature-modulated.

Graphical Abstract

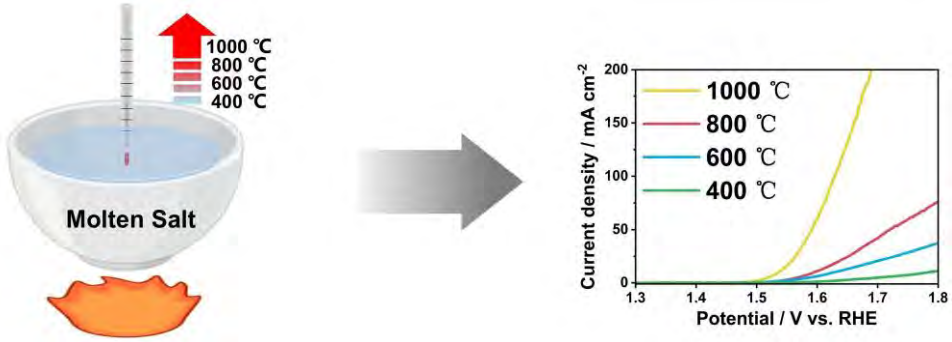

The oxygen evolution reaction (OER) involves a complex 4-electron transfer process with sluggish kinetics, significantly limiting the overall efficiency of water splitting.[1] Also, some noble-metal-based catalysts such as IrO_2 and RuO_2 are hindered from large-scale application due to their high cost and scarcity.[2] Therefore, the development of efficient, stable, and cost-effective OER catalysts is crucial to advance electrochemical hydrogen production technology, such as transition-metal-based materials.[3] Among them, FeNi bimetallic/carbon composite systems have gained significant attention due to their synergistic electronic interactions, earth abundance, and high intrinsic activity in alkaline electrolytes.[4] The molten salt (MS) synthesis method has emerged as an effective strategy for nanomaterial preparation, owing to its structural tunability brought about by its scalability and unique reaction environment that bridges the respective advantages of conventional solid and liquid-phase synthesis methods.[5] For example, high-entropy metal oxide,[6] 2D transition-metal carbides,[7] single-atom catalysts,[8] etc., can be readily obtained by using MS assistance. For the synthesis of FeNi/carbon composites,

[Received on 21 May 2025; revised on 23 June 2025; accepted on 30 June 2025; corrected and typeset on 28 July 2025]

eutectic salt medium not only serves as a reaction environment that enables homogeneous diffusion and accelerates the ion-transfer rate, but also prevents severe particle agglomeration. Moreover, when a carbon source such as glucose is added during the process, it can form a conductive and porous carbon substrate, promoting electrical conductivity. However, the effect of the synthesis temperature on the structure–performance relationship of MS-derived metal/carbon catalysts requires further investigation.

In this work, we employed a LiCl–KCl MS-assisted strategy to synthesize FeNi/carbon (denoted as FNC-X, where X represents the synthesis temperature: 400, 600, 800, and 1,000 °C), aiming to explore how temperature modulation during synthesis influences the electrochemical performance. Here, $FeCl_2{\cdot}4H_2O$ and $NiCl_2{\cdot}6H_2O$ were used as metal precursors and glucose was employed as a carbon source. A eutectic mixture of LiCl and KCl was used as the MS due to the low melting point (357 °C), enabling the study of the carbonization of glucose. During the calcination process, glucose undergoes thermal decomposition to generate carbon, which provides a reductive environment and effectively reduces Fe^{2+} and Ni^{2+} ions to their metallic states. Meanwhile, the MS provided an ion-conducting environment that promotes metal-ion diffusion. These combined effects enable the formation of FeNi alloy dispersed on the carbon substrate, without the need for additional chemical reducing agents. A systematic characterization was carried out to investigate the influence of the annealing temperature on the morphology evolution, crystal structure, specific surface area, surface composition, and electrochemical performance. Our results reveal that increasing the calcination temperature leads to enhanced graphitization and the formation of larger FeNi particles. Notably, when compared with the electrocatalyst fabricated at lower temperatures, the sample synthesized at 1,000 °C exhibited the best OER performance with the lowest overpotential of 306.7 mV at a current density of 10 mA cm^{-2}, the smallest Tafel slope of 62.1 mV dec^{-1}, and a stability test for 100 h, attributed to its high conductivity, the balance of graphitization and defects that form on the carbon substrate, the larger surface area, and the optimal surface electronic states of Fe and Ni. This work highlights the advantages of temperature regulation in MS-synthesized OER catalysts and provides new insights into the design of high-performance electrocatalysts based on transition metals.

The morphology of FNC-X with different annealing temperatures was investigated by scanning electron microscopy (SEM). As shown in Fig. 1a, the glucose has been carbonized, resulting in a relatively smooth surface for FNC-400. A polymer-like network was observed and no 2D layer-like structure appeared, hinting at the low degree of crystallization in the carbonization. When the temperature increases to 600 °C (Fig. 1b), the surface becomes rougher, accompanied by the disappearance of the polymer-like network structure. Instead, the carbon substrate appears as a block-like and porous structure. As the synthesis temperature is further increased to 800 °C (Fig. 1c), a highly porous structure consisting of stacked small carbon sheets is observed, suggesting the onset of the reorganization and graphitization of the carbon substrate when the temperature rises. As shown in Fig. 1d, it can be seen that, when the synthesis temperature was increased to 1,000 °C, the obtained carbon sheets appeared to be thinner and larger, demonstrating the growth of the graphene-like layer. This morphological evolution is caused

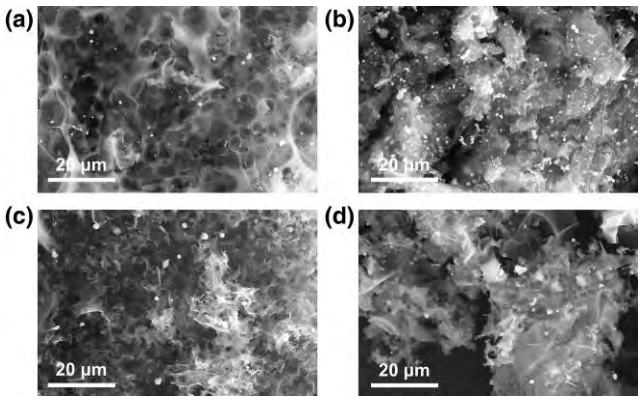

Fig. 1. SEM images of a) FNC-400; b) FNC-600; c) FNC-800; d) FNC-1000.

by the dehydration of the glucose in the eutectic salt solvent and secondary growth through high-temperature calcination, which are beneficial for increasing the specific surface area of the catalyst.[9] The Brunauer–Emmett–Teller method was further applied to measure the specific surface area of the as-prepared samples. As shown in Supplementary Table S1, the surface area increases from 88.3 m^2 g^{-1} for FNC-400 to 336.6 m^2 g^{-1} for FNC-1000, which is attributed to the development of a porous carbon substrate and the formation of large graphene-like sheets in the high-temperature MS environment. A higher surface area not only provides more active sites, but also promotes electrolyte penetration and gas diffusion during the OER process.[10]

In addition to the evolution of the carbon substrate, the size of the metal particles also changes significantly with the calcination temperatures. For FNC-400 and FNC-600, smaller metal particles are observed. On the other hand, the metal nanoparticles of FNC-800 and FNC-1000 exhibit a larger size. Transmission electron microscopy (TEM) images were further used to investigate the size of the metallic nanoparticles (Supplementary Fig. S1). As the synthesis temperature increases, the FeNi particle size shows an obvious growth trend. The average particle sizes for FNC-400, FNC-600, FNC-800, and FNC-1000 are 0.33 ± 0.29, 1.01 ± 0.33, 1.15 ± 0.38, and 1.55 ± 0.91, respectively. This increase in the particle diameter can be attributed to the accelerated ion mobility and thermal sintering effects at higher temperatures, which promote the merging of small nanoparticles into larger ones.[11] TEM-energy-dispersive X-ray spectroscopy (EDS) was performed to reveal the elemental distribution of FNC-1000. As shown in Supplementary Fig. S2, the EDS mapping demonstrates a uniform distribution of Ni and Fe in the particle, indicating the successful formation of the FeNi alloy. The Ni/Fe atomic ratios were evaluated by using SEM-EDS, as shown in Supplementary Table S2. All samples exhibit a relatively consistent Ni Fe atomic ratio close to 5:1, which is consistent with the molar ratio of the metal precursors.

The crystal structures of FNC-X were characterized by using X-ray diffraction (XRD), as shown in Fig. 2a. All samples exhibit 3 diffraction peaks located at around 44.4°, 51.6°, and 76.1°, which can be attributed to the (111), (200), and (220) crystal planes of the face-centered cubic phase of the FeNi alloy (PDF#01-071-832).[12] The FeNi alloy peaks also exist in FNC-400, suggesting that the alloy phase can be formed at a relatively low heating temperature under the MS-assisted

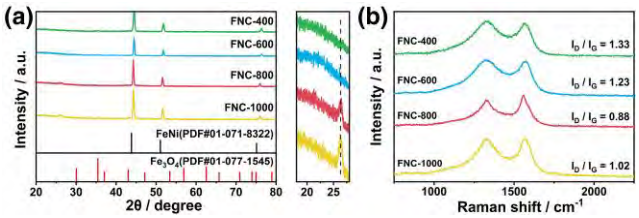

Fig. 2. a) XRD patterns of FNC-X; b) Raman spectra of FNC-X.

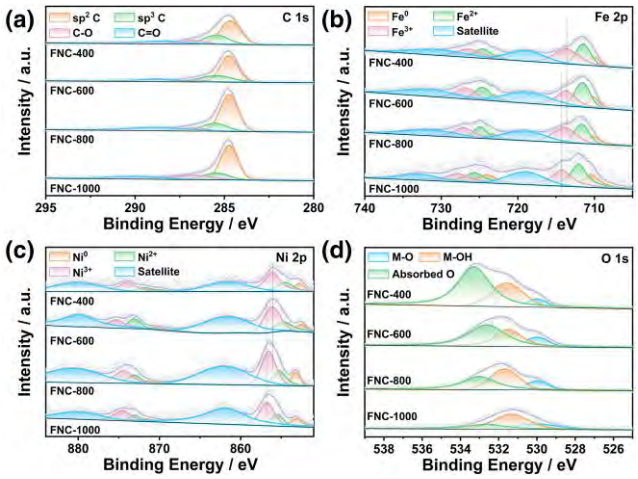

Fig. 3. High-resolution XPS spectra of FNC-X. a) C 1s; b) F 2p; c) Ni 2p; d) O 1s.

synthesis conditions. Additionally, a weak and broad peak at around 21.8° is observed for FNC-400 and FNC-600, which corresponds to the amorphous carbon structure. When the annealing temperature increases to 800 °C and 1,000 °C, the (002) diffraction peak of carbon at 26.4° becomes sharper, suggesting the transition from a disordered carbon phase to a graphitic state.[13] These results demonstrate that increasing the reaction temperature facilitates the graphitization of the carbon substrate, which is beneficial for enhancing the electrical conductivity.

Raman spectroscopy was employed to further evaluate the degree of graphitization and structural defects of the carbon substrate of FNC-X, as shown in Fig. 2b. All samples display 2 characteristic peaks: one being the D band and another being the G band. The D band located at 1,330 cm^{-1} corresponds to the disordered carbon, while the G band located at 1,564 cm^{-1} corresponds to the graphitic carbon caused by the in-plane vibration of sp^2 hybridized carbon.[14] The ratio of the intensities of the D band and the G band (I_D/I_G) is used to investigate the defect and the degree of graphitization. The I_D/I_G values of FNC-400, FNC-600, FNC-800, and FNC-1000 are 1.33, 1.23, 0.88, and 1.02, respectively. The higher I_D/I_G ratios for FNC-400 and FNC-600 suggest that the carbon substrate exhibits an amorphous structure at lower calcination temperatures. With the increase in the heating temperature to 800 °C, the I_D/I_G value decreases to 0.88, indicating an increase in the degree of graphitization and structural order. It is consistent with the carbon sheet stacking observed in the SEM image and the sharper carbon diffraction peak in the XRD pattern, suggesting that the carbon structure has a transition from disorder to crystallization with the increasing annealing temperature. However, a slight increase in the intensity of I_D/I_G to 1.02 is found for FNC-1000, which is due to the formation of new edge defects during the high-temperature treatment. The similar intensities of the D band and the G band indicate a balance between defects and graphitization, which not only increases the formation of active sites, but also improves the conductivity of the catalyst.[15]

X-ray photoelectron spectroscopy (XPS) was employed to analyze the surface elemental composition and electronic state of FNC-X, as shown in Supplementary Table S3 and Fig. 3. In Supplementary Table S3, the carbon to metal atomic ratio for all samples remains at around 50:1, which is consistent with the structural design of the FeNi alloy nanoparticles distributed on the carbon substrate. In the C 1s XPS high-resolution spectrum (Fig. 3a), all samples exhibit 4 deconvoluted peaks assigned to sp^2 carbon at 284.7 eV, sp^3 carbon at 285.5 eV, C–O at 286.7 eV, and C=O at 288.8 eV, respectively.[16] Notably, from Supplementary Table S4, the area ratio of sp^2/sp^3 increases with the increasing pyrolysis temperature from 400 °C to 1,000 °C, rising from 2.14 (FNC-400) to 3.54 (FNC-1000). The increased sp^2 C content indicates an enhancement in the degree of graphitization at higher synthesis temperatures, which not only enhances the crystal qualities of the carbon substrate, but also improves the electrical conductivity and accelerates the charge transfer in the OER. The Fe 2p spectra display the coexistence of the metallic Fe at 710.0 to 710.4 eV for $2p_{3/2}$ and 722.8 to 724.0 eV for $2p_{1/2}$, the oxidation states of Fe^{2+} at 711.5 to 712.0 eV for $2p_{3/2}$ and 722.8 to 724.0 eV for $2p_{1/2}$, as well as the Fe^{3+} at 713.6 to 714.3 eV for $2p_{3/2}$ and 726.3 to 727.8 eV for $2p_{1/2}$ (Fig. 3b).[17] Similarly, the Ni 2p spectra show 3 main peaks for Ni $2p_{1/2}$ and $2p_{3/2}$, corresponding to Ni^0 at 852.6 to 853.1 eV and 870.0 to 871.6 eV, Ni^{2+} at 854.5 to 855.5 eV and 871.8 to 873.1 eV, and Ni^{3+} at 856.0 to 856.8 eV and 874.0 to 875.3 eV (Fig. 3c).[18] As shown in Supplementary Tables S5 and S6, both peaks representing the Fe^{3+} and Ni^{3+} states shift toward higher binding energies with the increasing synthesis temperatures due to stronger interactions between the metal and the substrate. From previous literature, it is known that the high valence states of transition metals (Fe^{3+} and Ni^{3+}) can facilitate the formation and participation of key intermediates in OER, particularly OOH species, and may promote OER kinetics via lattice oxygen oxidation mechanisms.[19] Meanwhile, the relative content of the Fe^0 peak obviously increases from 10.9% in FNC-400 to 23.3% in FNC-1000, and Ni^0 increases from 11.5% to 19%, indicating a temperature-induced reduction environment within the MS that promotes the reduction of Fe and Ni species. These results correspond to the TEM images, which confirm the formation of FeNi alloy in all samples and the growth of metal particles at high annealing temperatures. The O 1s spectra (Fig. 3d) can be fitted into 3 main peaks: lattice oxygen (M–O) located at 530.2 eV, hydroxyl species (M–OH) located at 531.8 eV, and adsorbed H_2O located at 533.5 eV.[20] FNC-1000 shows a higher relative content of M–O and M–OH species (Supplementary Table S7), which suggests the presence of stable surface oxides that may contribute to improving electrocatalytic activity. These results confirm that the surface electronic structure of FNC-X can be effectively tuned via the temperature modulation of MS synthesis, optimizing redox synergy and charge-transfer kinetics.

Considering the significant structural and surface chemical evolution observed with increasing synthesis temperature, it

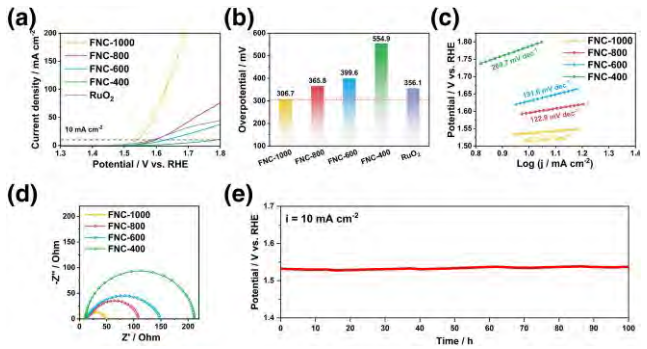

Fig. 4. Electrochemical performance of as-prepared samples and RuO_2. a) Polarization curves; b) overpotentials at 10 mA cm^{-2}; c) Tafel slope; d) electrochemical impedance spectra; e) stability test.

is important to investigate the effects of these changes on the OER activity of FNC-X. Therefore, the electrocatalytic activities of FNC-X in 1 M KOH electrolyte were systematically investigated, as shown in Fig. 4. From Fig. 4a and b, it can be seen that FNC-1000 exhibits the lowest overpotential of 306.7 mV at a current density of 10 mA cm^{-2} among all the synthesized catalysts, even outperforming the benchmark RuO_2 catalyst (356.1 mV). In contrast, the sample prepared at lower temperatures shows higher overpotentials at 10 mA cm^{-2}: FNC-800 (365.8 mV), FNC-600 (399.6 mV), and FNC-400 (554.9 mV). This demonstrates that high-calcination-temperature treatment can enhance the electrocatalytic activity of the FNC sample for the OER. Tafel plots derived from the linear sweep voltammetry curves (Fig. 4c) further support this. FNC-1000 exhibits the smallest Tafel slope value of 62.1 mV dec^{-1}, suggesting faster OER kinetics compared with FNC-800 (122.9 mV dec^{-1}), FNC-600 (191.6 mV dec^{-1}), and FNC-400 (269.7 mV dec^{-1}). To evaluate the charge-transfer rate of FNC-X, electrochemical impedance spectroscopy was conducted and the corresponding Nyquist plots are shown in Fig. 4d. FNC-1000 shows a smaller charge-transfer resistance (Rct) of 39 Ω than FNC-400 (201 Ω), FNC-600 (140 Ω), and FNC-800 (98 Ω). This suggests superior electrical conductivity and more efficient electron transfer during the OER, which is attributed to the conductive graphitic carbon substrate and sufficient active site exposure. The durability of FNC-1000 was confirmed by chronopotentiometry measurement at 10 mA cm^{-2} in 1.0 M KOH electrolyte (Fig. 4e). FNC-1000 maintains a stable potential over 100 h, indicating excellent stability. Compared with previously reported transitional metal-based OER catalysts, FNC-1000 exhibits superior performance in activity and stability (Supplementary Table S8). In summary, FNC-1000 exhibits the best OER performance among all the synthesized samples, which proves that a higher annealing temperature significantly improves the electrochemical performance.

In this work, FeNi/C electrocatalysts were successfully synthesized by using an MS-assisted method at different temperatures. With an increase in the synthesis temperature from 400 °C to 1,000 °C, the carbon substrate evolves from an amorphous to a graphitic state and, from 800 °C to 1,000 °C, new defects are introduced, and larger and thinner graphite sheets are generated. This not only improves the conductivity, but also increases the specific surface area of the catalyst. At the same time, the alloy particle size gradually increases and the optimized surface state is formed, which is beneficial for the OER. As a result, FNC-1000 exhibits the best OER performance among all the samples with the lowest overpotential of 306.7 mV at a current density of 10 mA cm^{-2}, the smallest Tafel slope of 62.1 mV dec^{-1}, and 100 h of stable performance, attributed to its favorable structural and surface state. This work provides valuable insights into the design of efficient bimetallic alloy/carbon-based electrocatalysts by using MS synthesis and emphasizes the critical role of the synthesis temperature in improving catalytic activity.

Author contributions

X.L. designed the experiments and synthesized the samples. X.L. and D.S. preformed the electrochemical measurements and the characterizations. X.L. wrote the manuscript. X.L., D.S., and L.D. analyzed the data. T.Y., J.C.H., and S.Y. directed this work. All authors discussed and revised the manuscript.

Supplementary data

Supplementary material is available at *Chemistry Letters* online.

Funding

This work was funded by the Network Joint Research Center for Materials and Devices of the Ministry of Education, Culture, Sports, Science and Technology (MEXT). The first author was supported by the China Scholarship Council (CSC).

Conflict of interest statement. None declared.

References

1. K. Zeng, D. Zhang, *Prog. Energy Combust. Sci.* **2010**, *36*, 307. https://doi.org/10.1016/j.pecs.2009.11.002
2. C. C. McCrory, S. Jung, I. M. Ferrer, S. M. Chatman, J. C. Peters, T. F. Jaramillo, *J. Am. Chem. Soc.* **2015**, *137*, 4347. https://doi.org/10.1021/ja510442p
3. E. Fabbri, A. Habereder, K. Waltar, R. Kötz, T. J. Schmidt, *Catal. Sci. Technol.* **2014**, *4*, 3800. https://doi.org/10.1039/C4CY00669K
4. M. Wu, B. Guo, A. Nie, R. Liu, *J. Colloid Interface Sci.* **2020**, *561*, 585. https://doi.org/10.1016/j.jcis.2019.11.033
5. D. Chen, S. Mu, *Adv. Mater.* **2024**, *36*, 2408285. https://doi.org/10.1002/adma.202408285
6. D. Song, X. Liu, Y. Wu, Q. Quan, Y. Tsuji, X. Liu, H. Saito, S. Ihara, L. Dai, X. Liang, T. Yanagida, *J. Mater. Chem. A* **2025**, *13*, 13295. https://doi.org/10.1039/D4TA08485C
7. J. Wu, J. Su, T. Wu, L. Huang, Q. Li, Y. Luo, H. Jin, J. Zhou, T. Zhai, D. Wang, Y. Gogotsi, *Adv. Mater.* **2023**, *35*, e2209954. https://doi.org/10.1002/adma.202209954
8. M. Xiao, L. Zhang, B. Luo, M. Lyu, Z. Wang, H. Huang, S. Wang, A. Du, L. Wang, *Angew. Chem.* **2020**, *132*, 7297. https://doi.org/10.1002/ange.202001148
9. X. Liu, C. Giordano, M. Antonietti, *Small* **2014**, *10*, 193. https://doi.org/10.1002/smll.201300812
10. L. Xu, Q. Jiang, Z. Xiao, X. Li, J. Huo, S. Wang, L. Dai, *Angew. Chem.* **2016**, *128*, 5363. https://doi.org/10.1002/ange.201600687
11. E. Ruckenstein, B. Pulvermacher, *J. Catal.* **1973**, *29*, 224. https://doi.org/10.1016/0021-9517(73)90226-1

12. U. Y. Qazi, C.-Z. Yuan, N. Ullah, Y.-F. Jiang, M. Imran, A. Zeb, S.-J. Zhao, R. Javaid, A.W. Xu, *ACS Appl. Mater. Interfaces* **2017**, *9*, 28627. https://doi.org/10.1021/acsami.7b08922
13. X. Zheng, J. Deng, N. Wang, D. Deng, W.-H. Zhang, X. Bao, C. Li, *Angew. Chem. Int. Ed. Engl.* **2014**, *53*, 7023. https://doi.org/10.1002/anie.201400388
14. M. Roslan, K. Chaudary, Z. Haider, A. Zin, J. Ali, *Effect of magnetic field on carbon nanotubes and graphene structure synthesized at low pressure via arc discharge process*, AIP Conference Proceedings, AIP Publishing, Langkawi, **2017**.
15. Z. Liu, X. Yu, H. Yu, H. Xue, L. Feng, *ChemSusChem* **2018**, *11*, 2703. https://doi.org/10.1002/cssc.201801250
16. B.-J. Kim, J.-P. Kim, J.-S. Park, *Nanoscale Res. Lett.* **2014**, *9*, 236. https://doi.org/10.1186/1556-276X-9-236
17. S.-Y. Lin, X. Zhang, S.-Y. Sang, L. Zhang, J.-J. Feng, A.-J. Wang, *J. Coll. Interface Sci.* **2022**, *628*, 499. https://doi.org/10.1016/j.jcis.2022.07.180
18. Z. Xu, G. Chen, F. Yang, J. Jang, G. Liu, F. Xiao, Y. Sun, X. Qiu, W. Chen, D. Su, M. Gu, M. Shao, *Electrochim. Acta* **2023**, *458*, 142549. https://doi.org/10.1016/j.electacta.2023.142549
19. D. Qi, X. Chen, W. Liu, C. Liu, W. Liu, K. Wang, K. Wang, J. Jiang, *Inorg. Chem. Front.* **2020**, *7*, 642. https://doi.org/10.1039/C9QI01325C
20. G. Zhang, J. Zeng, J. Yin, C. Zuo, P. Wen, H. Chen, Y. Qiu, *Appl. Catal. B* **2021**, *286*, 119902. https://doi.org/10.1016/j.apcatb.2021.119902